Published in final edited form as:
Mol Microbiol. 2012 April ; 84(1): 66–76. doi:10.1111/j.1365-2958.2012.08009.x.

TcdB from Hypervirulent *Clostridium difficile* Exhibits Increased Efficiency of Autoprocessing

Jordi M. Lanis[1], **Logan D. Hightower**[1], **Aimee Shen**[2], and **Jimmy D. Ballard**[1]

[1]Department of Microbiology and Immunology, University of Oklahoma Health Sciences Center, Oklahoma City, OK 73104

[2]University of Vermont, Microbiology and Molecular Genetics, Burlington, VT 05045

Summary

TcdB, an intracellular bacterial toxin that inactivates small GTPases, is a major *Clostridium difficile* virulence factor. Recent studies have found that TcdB produced by emerging/hypervirulent strains of *C. difficile* is more potent than TcdB from historical strains, and in the current work, studies were performed to investigate the underlying mechanisms for this change in TcdB toxicity. Using a series of biochemical analyses we found that TcdB from a hypervirulent strain ($TcdB_{HV}$) was more efficient at autoprocessing than TcdB from a historical strain ($TcdB_{HIST}$). $TcdB_{HV}$ and $TcdB_{HIST}$ were activated by similar concentrations of IP6; however, the overall efficiency of processing was 20% higher for $TcdB_{HV}$. Using an activity based fluorescent probe (AWP19) an intermediate, activated but uncleaved, form of $TcdB_{HIST}$ was identified, while only a processed form of $TcdB_{HV}$ could be detected under the same conditions. Using a much higher concentration (200 μM) of the probe revealed an activated uncleaved form of $TcdB_{HV}$, indicating a preferential and more efficient engagement of intramolecular substrate than $TcdB_{HIST}$. Futhermore, a peptide-based inhibitor (Ac-GSL-AOMK), was found to block the cytotoxicity of $TcdB_{HIST}$ at a lower concentration than required to inhibit $TcdB_{HV}$. These findings suggest that $TcdB_{HV}$ may cause increased cytotoxicity due to more efficient autoprocessing.

Keywords

Clostridium difficile; Toxin B; NAP1; cysteine protease

INTRODUCTION

Clostridium difficile-associated disease (CDAD) is a serious health care problem for hospitalized patients and elderly patients in long-term nursing facilities (McFarland *et al.*, 1989; Simor *et al.*, 1993; Bartlett, 1992; Redelings *et al.*, 2007; Gerding, 2010). The disease has also recently emerged in healthy individuals within the general population (Klein *et al.*, 2006; Hirschhorn *et al.*, 1994; Wilcox *et al.*, 2008; CDC, 2008). In a common scenario, CDAD occurs when patients undergoing antibiotic treatments are infected with spores of *C. difficile* residing within the hospital (McFarland *et al.*, 1989). It is thought that spores enter the new host by ingestion, survive the stomach's acidic environment, and then germination is triggered by bile salts (Sorg and Sonenshein, 2008; Wilson *et al.*, 1985; Wilson, 1983), although many details of this infection need further investigation. After germination, *C. difficile* colonizes the large intestines and releases toxins that cause localized inflammation

*Address correspondence to: Jimmy D. Ballard, Ph.D., The University of Oklahoma Health Sciences Center, Department of Microbiology and Immunology, BRC-358, 975 NE 10th Street, Oklahoma City, OK 73104. Phone: 405-271-3855. Fax 405-271-3874. jimmy-ballard@ouhsc.edu.

and then systemic damage (Sullivan *et al.*, 1982; Taylor *et al.*, 1981; Abrams *et al.*, 1980; Hamm *et al.*, 2006; Libby *et al.*, 1982). Thus, the activity of *C. difficile* toxins influences the outcome of CDAD.

CDAD frequency, severity, and mortality have increased over the past decade. A recent report by Karas *et al.* found a striking difference in the mortality rate prior to and following the year 2000 (Karas *et al.*, 2010). Before 2000 the mortality rate of CDAD patients was estimated to be 3.64% and after 2000 the mortality rate increased to over 8.0% (Redelings *et al.*, 2007). The increases in disease severity, frequency, and mortality are directly correlated with emergence of a hypervirulent strain of *C. difficile* termed North American Pulsovar 1 (NAP1), Restriction Endonuclease Assay Type BI, and Ribotype 027 *C. difficile* strain (referred to as *C. difficile* NAP1 herein) (McDonald *et al.*, 2005; Muto *et al.*, 2005). *C. difficile* NAP1 may exhibit several characteristics that could explain the strain's role in increasing the morbidity and mortality of this disease. *C. difficile* NAP1 is fluoroquinolone resistant, and some groups have proposed these strains sporulate more efficiently than historical strains, and possibly express higher levels of the two major *C. difficile* toxins (TcdA and TcdB) (Akerlund *et al.*, 2008; Bourgault *et al.*, 2006; Drudy *et al.*, 2006; Drudy and Kyne, 2007; Warny *et al.*, 2005; Merrigan *et al.*, 2010). Additionally, recent reports by us and others have revealed that TcdB expressed by *C. difficile* NAP1 ($TcdB_{HV}$) is more cytotoxic than TcdB from a historical strain of *C. difficile* ($TcdB_{HIST}$) (Stabler *et al.*, 2009; Lanis *et al.*, 2010). Many of the properties originally attributed to the increased virulence of the NAP1 strains are controversial, as recent reports suggest neither sporulation characteristics nor toxin levels correlate with hypervirulent strain type or clade (Carter *et al.*, 2011; Burns *et al.*, 2011). Thus, increased toxicity of $TcdB_{HV}$ is a reasonable explanation, at least in part, for the heightened virulence of hypervirulent strains of *C. difficile*.

TcdB (~270 kD) is an intracellular bacterial toxin that glucosylates small GTPases from the Rho family of proteins (Just *et al.*, 1995). TcdB is thought to engage a yet undefined cell surface receptor and enter the cell via receptor-mediated endocytosis; acidification of the endosome and formation of ion-conducting channels occur during cell entry by TcdB (Florin and Thelestam, 1986; Florin and Thelestam, 1983; Qa'Dan *et al.*, 2000; Barth *et al.*, 2001; Papatheodorou *et al.*, 2010; von Eichel-Streiber *et al.*, 1992). Upon exposure to the cytoplasm TcdB binds inositol hexakisphosphate (IP6), which activates the toxin's intramolecular cysteine protease domain (CPD) (Reineke *et al.*, 2007; Egerer *et al.*, 2007; Egerer *et al.*, 2009). Following autoprocessing by the CPD, the glucosyltransferase domain is released into the cytoplasm where it inactivates target substrates (Reineke *et al.*, 2007; Rupnik *et al.*, 2005; Pfeifer *et al.*, 2003). In a previous study we reported that $TcdB_{HV}$ entered cells rapidly and proposed that $TcdB_{HV}$ may be translocated into the cytosol at an earlier stage of endosomal trafficking than $TcdB_{HIST}$ (Lanis *et al.*, 2010). Accelerated cell entry by $TcdB_{HV}$ was congruent with our observation that $TcdB_{HV}$ undergoes a hydrophobic transition at a higher pH than $TcdB_{HIST}$ (Lanis *et al.*, 2010). Such a pH-induced structural change has previously been shown to be a prelude to membrane insertion by TcdB (Qa'Dan *et al.*, 2000; Barth *et al.*, 2001). Whether autoprocessing of $TcdB_{HV}$ might also be activated more quickly or efficiently by IP6 is not known, but such a phenotype would support a model in which $TcdB_{HV}$ can enter cells more rapidly than $TcdB_{HIST}$.

In the current study we were interested in knowing if the previously observed $TcdB_{HV}$ phenotypes were related to highly efficient autoprocessing. The findings from this study support this notion and provide insight into a mechanism underlying the heightened toxicity of TcdB produced by a hypervirulent strain of *C. difficile*.

RESULTS

Comparison of $TcdB_{HV}$ and $TcdB_{HIST}$ Autoprocessing

We have reported previously that $TcdB_{HV}$ is able to undergo pH-induced hydrophobic transitions at a higher pH than $TcdB_{HIST}$ (Lanis *et al.*, 2010). This allows $TcdB_{HV}$ to translocate into the cytoplasm at an earlier stage of endocytosis, as we confirmed using a chase experiment involving lysosomotropic inhibitors (Lanis *et al.*, 2010). Yet, a conundrum of this observation is that earlier translocation into the cytoplasm should only increase the rate of intoxication, not the extent of cytotoxicity of $TcdB_{HV}$. This led us to investigate other activities related to cell entry that might be enhanced or more efficient in $TcdB_{HV}$.

Autoproteolytic activity could be a critical step in cell entry, and as such, differences in this activity between $TcdB_{HV}$ compared to $TcdB_{HIST}$ might contribute to variations in cytotoxicity. We first performed an experiment to determine if $TcdB_{HV}$ and $TcdB_{HIST}$ differed in their sensitivity to activation by IP6. The two forms of TcdB were incubated with IP6, ranging in concentration from 500 nM to 500 μM. The toxins were allowed to incubate with the various concentrations of IP6 for 1 h and the reaction was resolved by SDS-PAGE. The results from this comparison are shown in Fig. 1A. Autoprocessing of $TcdB_{HV}$ and $TcdB_{HIST}$ was activated by similar concentrations of IP6, with an EC_{50} of 8.2 ± 1.9 μM and 4.7 ± 0.9 μM of IP6 respectively (Fig. 1B). These concentrations are comparable to the reported binding constant of IP6 at 2 μM (Egerer *et al.*, 2009), and since intracellular concentrations of IP6 typically exceed 50 μM, the minor differences in sensitivity to IP6 most likely do not account for the variation in toxicity between $TcdB_{HV}$ and $TcdB_{HIST}$ (Irvine *et al.*, 2001).

Although we did not detect a significant difference in minimal concentrations of IP6 needed to activate $TcdB_{HV}$ compared to $TcdB_{HIST}$, we did note that a higher percentage of total $TcdB_{HV}$ protein was processed under these conditions. To examine this phenotype further, in the next experiment the two forms of TcdB were incubated with 100 μM IP6 (a condition of excess IP6) and the extent of processing was determined at time-points between 1 min and 60 min by using densitometry to quantify the relative amounts of processed and unprocessed toxin. As shown in Fig. 1C, $TcdB_{HV}$ underwent almost 80% cleavage within the first hour of incubation. In contrast, maximal processing of $TcdB_{HIST}$ is under 60%. This difference in percent autoprocessing does not seem to be due to the rate of activation, as both toxins reached the half-maximal level of proteolysis by 2 min (Fig. 1C). Finally, we wanted to confirm that these were universal differences in CPD activity between $TcdB_{HIST}$ and $TcdB_{HV}$ and not a function of experimental conditions. Dithiothreitol (DTT) has also been shown to activate processing of TcdB, and in Fig. 1D the in vitro cleavage reaction has been repeated on $TcdB_{HIST}$ and $TcdB_{HV}$ using 5 mM DTT in place of IP6. While DTT is not as efficient an activator of proteolysis as IP6, the data indicate that DTT-mediated activation was substantially more efficient for $TcdB_{HV}$ in comparison to $TcdB_{HIST}$. We examined this difference over a time-course of 90 min, and while $TcdB_{HV}$ was activated by DTT within 15 min and reached maximum activation within approximately 1 h, the activation of $TcdB_{HIST}$ by DTT during this time-course was just slightly above the level of detection (Fig. 1D). These data indicate that $TcdB_{HV}$ is more efficient than $TcdB_{HIST}$ in autoproteolytic processing, and that these differences are independent of rate and interaction with IP6.

Probing the Activation State of $TcdB_{HV}$ and $TcdB_{HIST}$ using an Activity-Based Fluorescent Probe

Previous work by Puri *et al.* described a fluorescent small molecule designed to interact with TcdB when the CPD domain has been activated (Puri *et al.*, 2010). This probe is

fluorescently labeled SL-AOMK that was designed from a peptide-based Ac-GSL-AOMK protease inhibitor and can interact with the protease domain by mimicking the natural substrate and binding covalently to the catalytic cysteine. The probe (AWP19) depends on availability of the active site to bind; therefore, AWP19 is a useful tool to compare the IP6 induced conformational changes and subsequent activation of the CPD between $TcdB_{HIST}$ and $TcdB_{HV}$ (Puri *et al.*, 2010). Further work by Shen *et al.* demonstrated that this probe (AWP19) could be used to precisely measure the kinetics and substrate binding characteristics of the TcdB-CPD active site (Shen *et al.*, 2011). Using a FITC conjugated version of AWP19, we examined the differences in IP6-induced changes to the active site between $TcdB_{HIST}$ and $TcdB_{HV}$. In this experiment, both forms of TcdB were incubated with a range of IP6 concentrations and, following a 1 h incubation, AWP19 was added in 10-fold molar excess to the proteins. The reactions were then resolved by SDS-PAGE and the extent of labeling at each concentration of IP6 was determined by scanning for FITC fluorescence. As shown in Fig. 2A, both $TcdB_{HIST}$ and $TcdB_{HV}$ labeled with AWP19 could be detected following incubation with 5 μM IP6, although the level of labeled protein at this concentration was substantially less than that observed at higher concentrations of IP6. Densitometry of gels from 4 independent experiments using different toxin preparations indicates that the total labeling of $TcdB_{HV}$ is much higher than $TcdB_{HIST}$, however, equal amounts of IP6 are required for half-maximal activity of both toxins (Fig 2B). The predominant labeling of TcdB by AWP19 is observed in the $TcdB_{544\text{-}2366}$ fragment, indicating that the probe is only able to detect processed toxin under these conditions. Therefore, the difference in AWP19 labeling between the toxin variants can be attributed to the difference in maximal proteolysis between $TcdB_{HIST}$ and $TcdB_{HV}$, consistent with the findings in Fig 1A.

To continue utilizing the probe as an indicator of differential CPD activity, our next experiments concentrated on validating whether the probe interacts with equal affinity to both $TcdB_{HIST}$ and $TcdB_{HV}$. To this end, 0.3 μM of toxin was incubated with or without 100 μM IP6, then AWP19 was added from 0.3 μM up to 300 μM. The samples were analyzed by SDS-PAGE for FITC fluorescence and the percent processing by coomassie stain. As in previous experiments, $TcdB_{HV}$ exhibits greater fluorescence than $TcdB_{HIST}$ (Fig 3A). However, once the fluorescence is normalized by the percent of processing it is clear that the extent of labeling is nearly identical between the different strains of TcdB (Fig. 3B). Another concern was whether the probe could differentially bind to the CPD without activation by IP6. While a prolonged 24 hr incubation of either $TcdB_{HIST}$ or $TcdB_{HV}$ with AWP19 does lead to some minimal labeling (Fig. 3B), the level of detection is much lower than with activated CPD as determined by densitometry (Fig. 3C). These experiments validate that there is no differential affinity of AWP19 to either $TcdB_{HIST}$ or $TcdB_{HV}$, and the probe is a valuable tool for studying subtle differences in CPD activity between toxins.

We next used the AWP19 probe to examine activation of TcdB over a specific time-course. $TcdB_{HIST}$ or $TcdB_{HV}$ were incubated with IP6 and AWP19 simultaneously, and the level of activated protein was again determined by examining the extent of fluorescent protein resolved by SDS-PAGE. Interestingly, when IP6 and AWP19 were added to proteins at the same time, a full-length (unprocessed) form of $TcdB_{HIST}$ was detected. In contrast only the processed form of $TcdB_{HV}$ was detected in this assay and at a much later time-point (Fig. 4A).

We envisioned two possible explanations for detecting activated, but unprocessed, $TcdB_{HIST}$. First, the kinetics of autoproteolysis may occur in a manner slow enough to capture an intermediate form of $TcdB_{HIST}$, but occur much faster in $TcdB_{HV}$. Alternatively, the binding affinity for the intramolecular substrate could be stronger in $TcdB_{HV}$ than in $TcdB_{HIST}$, which would preclude competitive binding of AWP19 in $TcdB_{HV}$. Only after the

substrate has been cleaved could $TcdB_{HV}$ then bind the probe. We reasoned that if the latter was true, we should be able to detect the intermediate form of $TcdB_{HV}$ by adding higher concentrations of AWP19 to the reaction, thereby shifting the reaction to favor binding of the probe rather than the intramolecular domain. Therefore, we next assayed AWP19 labeling of TcdB under the conditions of an increasing ratio of probe to toxin. When $TcdB_{HIST}$ and $TcdB_{HV}$ were incubated with a 50-fold excess (20 μM) of AWP19 the full-length (unprocessed) form of $TcdB_{HV}$ could be detected (Fig. 4B). Further increases in probe concentration resulted in greater percentages of labeled full-length $TcdB_{HV}$ and a 500-fold excess (200 μM) shifted the predominant AWP19 labeling to the unprocessed form of $TcdB_{HV}$ (Fig. 4B–C). Additionally, the addition of excess probe can inhibit the processing of $TcdB_{HV}$, supporting the idea that the probe is outcompeting the intramolecular substrate for position in the active site (Fig. 4B inset). In contrast, AWP19 labeling of the processed form of $TcdB_{HIST}$ was much less evident under these conditions, consistent with the data in Fig. 4A, and the uncleaved form of the toxin was predominantly labeled under all probe concentrations (Fig. 4B–C).

Inhibition of Toxin function with the CPD inhibitor Ac-GSL-AOMK

The data thus far indicated that the entire cleavage process occurs much more efficiently in $TcdB_{HV}$, possibly due to an increased affinity for intramolecular substrate. To further investigate this process, we utilized a chemical inhibitor, previously described by Puri *et al.* (Puri *et al.*, 2010), to inhibit the CPD. We reasoned that a greater processing efficiency and a potential increased affinity to substrate in $TcdB_{HV}$ might affect the binding and inhibitory capacity of the CPD inhibitor. The toxins were pre-incubated with up to 100 μM of Ac-GSL-AOMK and then IP6 was added to 25 μM. Consistent with the difference in AWP19 labeling, we also observed a noticeable difference in the inhibition of processing between $TcdB_{HIST}$ and $TcdB_{HV}$. The difference in the concentration of inhibitor necessary to initiate blockage of IP6-induced processing of $TcdB_{HIST}$ or $TcdB_{HV}$ seems to be minimal, as evidence of inhibition was detectable in both toxins at concentrations around 12.5 μM Ac-GSL-AOMK (Fig. 5A). Densitometry of gels from 3 independent experiments revealed that the percent inhibition of $TcdB_{HV}$ reaches a maximum around 60% while nearly 100% of proteolysis is blocked in $TcdB_{HIST}$ (Fig. 5B). Just as AWP19 showed no effect in the absence of IP6, the inhibitor also had no effect on either $TcdB_{HIST}$ or $TcdB_{HV}$ without IP6 (data not shown), indicating that the inhibitor cannot bind in the absence of activation. Together, these experiments demonstrate that differences in proteolytic inhibition are not due to differential affinity or nonspecific binding of the inhibitor and support the interpretations from Fig. 4 in which $TcdB_{HV}$ has a structure that reduces such competitive binding of the inhibitor to the active site.

Next, we compared the inhibition of toxin function in a cell culture model. For these experiments, $TcdB_{HIST}$ and $TcdB_{HV}$ were pre-incubated with 100 μM of the inhibitor in media and the mixture added to CHO cells. Consistent with the in vitro data, we found that Ac-GSL-AOMK provided protection to $TcdB_{HIST}$ treated cells but was not as functional against $TcdB_{HV}$. Once toxin concentrations approach the TCD_{50} for $TcdB_{HV}$, the inhibitor is able to reduce cytopathic effects presumably because a 60% inhibition is sufficient at these low toxin levels. In comparison, the inhibitor prevented cytotoxicity of cells treated with 100-fold higher concentrations of $TcdB_{HIST}$ (Fig. 5C).

Discussion

In the current study we investigated the autoprocessing of TcdB from a hypervirulent strain of *C. difficile* and compared this with a well-studied form of TcdB from a historical strain. These data indicate $TcdB_{HV}$ autoprocessing occurs at a higher efficiency than autoprocessing by $TcdB_{HIST}$. Based on the earlier studies and the data presented in the

current work, a common theme has emerged. $TcdB_{HV}$ is more efficient during processes of cellular intoxication than $TcdB_{HIST}$ This important difference in the efficiency with which $TcdB_{HV}$ functions may be a fundamental determinant of the increased cytotoxicity of this toxin variant.

Not all large clostridial toxins (LCTs) appear to exhibit the same biochemistry and efficiency of autoprocessing, which supports the idea that $TcdB_{HIST}$ and $TcdB_{HV}$ could differ in their intramolecular proteolytic cleavage. For example, TcdA requires a much higher concentration of IP6 for activation compared to TcdB despite maintaining similar binding of IP6 (Egerer *et al*., 2007; Pruitt *et al*., 2009). Unlike other LCTs *Clostridium sordellii* lethal toxin (TcsL) requires a low pH for efficient autoprocessing (Guttenberg *et al.*, 2011). Interestingly, only full length TcsL required low pH for activation, while a recombinant fragment of just the glucosyltransferase and CPD domain did not (Guttenberg *et al*., 2011). These data suggest conformational differences encoded outside of the CPD influence the efficiency of autoprocessing, which is also a plausible explanation for the differences in the two forms of TcdB. In fact, this is the first study that utilizes native holotoxin to explore the function of the CPD in context of the full toxin molecule. Our data support the prediction that a structural difference impacts the variation in autoprocessing activity between $TcdB_{HV}$ and $TcdB_{HIST}$.

Results from the activation probe (AWP19) provide the basis for a model to explain differences in the efficiency of autoprocessing by $TcdB_{HIST}$ and $TcdB_{HV}$. The first major difference revealed by the studies using AWP19 is that $TcdB_{HIST}$ transitions from activated state to autocleavage more slowly than $TcdB_{HV}$. As shown in Fig. 4A, full-length unprocessed $TcdB_{HIST}$ was detected within less than a minute of addition of IP6, suggesting the protein was activated but had not yet engaged and cleaved intramolecular substrate. With extended IP6 incubation, $TcdB_{HIST}$ shifted to its processed form. In contrast, only trace levels of $TcdB_{HV}$ were detected in the unprocessed state following addition of IP6. Detection with AWP19 was substantially slower for $TcdB_{HV}$, but in contrast to $TcdB_{HIST}$ the prominent species found was the processed form of the toxin. An interpretation of these data is that $TcdB_{HV}$ is more efficient at autoprocessing because the protein is in a conformation that highly favors intramolecular substrate. Thus, limited detection of unprocessed $TcdB_{HV}$ can be explained by the fact that endogenous substrate blocks binding by AWP19 and only after cleavage is complete can the probe access the catalytic region. In contrast, $TcdB_{HIST}$ is less efficient at autoprocessing due to limitations in its capacity to interact with intramolecular substrate. This results in AWP19 competing with substrate and labeling the activated form $TcdB_{HIST}$.

The two strains of TcdB also demonstrate differential sensitivity to Ac-GSL-AOMK in the activation assay, and $TcdB_{HV}$ was much more resistant than $TcdB_{HIST}$ when the effects of the inhibitor were examined in a cellular intoxication assay. These results fit nicely with a model wherein subtle conformational differences account for the variation in autoprocessing. The CPD inhibitor, Ac-GSL-AOMK, is smaller in size than AWP19, which contains the bulkier FITC compound. Despite the smaller structure of Ac-GSL-AOMK access to the CPD is still restricted to activation by IP6 in both types of TcdB. How the inhibitor is able to effectively block $TcdB_{HIST}$ but not $TcdB_{HV}$ is related to the difference in binding of the AWP19 probe to the CPD. The probe has an equal affinity to both $TcdB_{HIST}$ and $TcdB_{HV}$ when the toxin has been pre-activated and normalized for the percent of processing. So, the difference in probe and inhibitor affinity to activated unprocessed toxin seems to be related to a difference in $TcdB_{HV}$ conformation that restricts binding to the CPD active site. The results of the inhibitor assays reveal another fundamental difference in the extent of toxic activity between $TcdB_{HIST}$ and $TcdB_{HV}$.

Variation in structure and function between $TcdB_{HIST}$ and $TcdB_{HV}$ could also have additional consequences on cytotoxicity, such as altering the way host cells defend against these toxins. S-nitrosylation of *C. difficile* toxins in vivo was recently reported by Savidge *et al.* as a host mechanism to inhibit toxin function (Savidge *et al.*, 2011). The authors found that IP6 and IP7 induced conformational changes to the toxin allowed for nitrosylation of the catalytic cysteine, leading to inhibition of toxin processing and a subsequent reduction in virulence (Savidge *et al.*, 2011). Our studies show that $TcdB_{HV}$ is processed much more efficiently, and also provide evidence that access to the catalytic cysteine is much more restricted than in $TcdB_{HIST}$. The way in which s-nitrothiols are able to interact with variants of TcdB inside the cell provide yet another explanation for the increased cytotoxicity of $TcdB_{HV}$.

$TcdB_{HIST}$ and $TcdB_{HV}$ exhibit differences in their primary sequence, rates of cell entry, efficiency of autoprocessing, and cytotoxicity. The findings to date all point to the fact that $TcdB_{HV}$ is more cytotoxic by virtue of some fundamental differences in the structure of this protein. An appealing model is one in which $TcdB_{HV}$ is a more flexible molecule than $TcdB_{HIST}$. Fig. 6 illustrates this model in which the increased flexibility of $TcdB_{HV}$ allows the toxin to more readily access intramolecular substrate. Therefore, this intramolecular interaction prevents binding to the probe or inhibitor until after the substrate has been cleaved. Conversely, $TcdB_{HIST}$ seems to maintain a structure that limits access of the CPD to the intramolecular substrate. In this way the interaction with the substrate is not sufficient to block binding by the probe and therefore the activated CPD can become labeled regardless of proteolysis (Fig. 6). This model supports the increased processing efficiency of $TcdB_{HV}$ and might also explain our previous observations on the extent of pH-induced conformational changes in $TcdB_{HV}$ (Lanis *et al.*, 2010). Further structural studies will be needed to refine this model and determine how sequence changes in $TcdB_{HV}$ influence the overall folding and induced conformational changes of this protein.

Experimental Procedures

Purification of Native TcdB

$TcdB_{HIST}$ and $TcdB_{HV}$ were isolated from *C. difficile* 10463 and *C. difficile* BI17 (provided by Dale Gerding) respectively, as previously described (Lanis *et al.*, 2010; Krivan and Wilkins, 1987; Qa'Dan *et al.*, 2000) The protein purity was assessed by SDS-PAGE, and the concentration determined by the Bradford method (Bio-Rad).

In vitro TcdB processing assays

The autoproteolysis assays were performed in 25 μl of 20 mM Tris-HCl pH 8.0, containing 2.5 μg of either $TcdB_{HIST}$ or $TcdB_{HV}$ and the indicated concentration of either Inositol hexakisphosphate (IP6), or dithiothreitol (DTT), to induce cleavage (all purchased from Sigma). Unless otherwise indicated, the samples were incubated at 37°C for 1 h, then boiled for 5 min in SDS sample buffer containing β-mercaptoethanol (BME) to halt the reaction. The samples were then separated by 8% SDS-PAGE and the toxin fragments visualized by coomassie blue stain.

Compound synthesis

FITC-AWP19 was synthesized by combining H_2N-aminohexanoic-SL-AOMK (1 equiv.) with 5(6)-Carboxyfluorescein N-hydroxysuccinimide ester (Sigma) and N,N-Diisopropylethylamine (Sigma) (5 equiv.) in DMSO for one hour and then purifying directly by HPLC. The identity and purity of the compound was characterized by LCMS.

AWP19 probe labeling of TcdB

For most of the experiments, processing of 0.3 μM $TcdB_{HIST}$ or $TcdB_{HV}$ was first stimulated with the indicated concentration of IP6 (Sigma) in 24 μl of 20 mM Tris-HCl, pH 8.0. The reaction was allowed to complete for 1h at 37°C, then AWP19 was added to a final concentration of 5 μM, bringing the total volume to 25 μl. The AWP19 labeling reaction was then continued at 37°C for one additional hour unless otherwise noted. 10 μl of SDS sample buffer containing BME was then added to the samples, and the samples were heated for 5 min at 95°C. 35 μl of each sample was resolved by 8% SDS-PAGE. Fluorescence of bands labeled by the AWP19-FITC probe was detected using an Alpha Innotech FluorChem Q imager, and then the gel was stained with coomassie to guarantee equal loading. For rate of AWP19 labeling experiments, 25 μM IP6 and 0.4 μM to 200 μM of AWP19 were added to 0.4 μM $TcdB_{HIST}$ or $TcdB_{HV}$ in 20 mM Tris-HCl, pH 8.0, simultaneously and incubated at 37°C for the time points indicated. The samples were then analyzed as described above.

Inactivation of TcdB with Ac-GSL-AOMK

The in vitro inhibition assays were performed in 25 μl of 20 mM Tris-HCl pH 8.0, containing 2.5 μg of either $TcdB_{HIST}$ or $TcdB_{HV}$ and up to 100 μM Ac-GSL-AOMK. The samples were incubated at 37°C for 30 min then IP6 (Sigma) was added to a final concentration of 25 μM. The reactions were incubated for 1 additional h at 37°C then heated for 5 min at 95°C in SDS sample buffer containing β-mercaptoethanol (BME) to halt the reaction. The samples were then separated by 8% SDS-PAGE and the toxin fragments visualized by coomassie blue stain.

To assess the inactivation of TcdB in cell culture, CHO-K1 cells (ATCC) were seeded in 96 well plates at a density of $1–2 \times 10^4$ cells per well in F12-K media (ATCC) supplemented with 10% FBS. Prior to the assay, 0.037, 0.37, or 3.7 pM $TcdB_{HIST}$ and $TcdB_{HV}$ were preincubated with 100 μM of the inhibitor Ac-GSL-AOMK for 30 min in 100 μl of F12-K media. 100 μl of this mixture was then added to each well in triplicate, and the cells were incubated at 37°C in the presence of 6% CO_2 for 24 hrs and cell viability was measured by CCK-8 (Dojindo).

Data Quantification and Non-linear Regression

Labeling and percent processing reactions were quantified using the program ImageJ (http://imagej.nih.gov/ij, NIH). The values were corrected for background and control and plotted against IP6 concentration, time, AWP19 concentration, or inhibitor concentration respectively. The graphs were curve-fit and the EC_{50} was determined using the Michaelis-Menten function on GraphPad Prism.

References

Abrams GD, Allo M, Rifkin GD, Fekety R, Silva J Jr. Mucosal damage mediated by clostridial toxin in experimental clindamycin- associated colitis. Gut. 1980; 21:493–499. [PubMed: 6776012]

Akerlund T, Persson I, Unemo M, Noren T, Svenungsson B, Wullt M, Burman LG. Increased sporulation rate of epidemic *Clostridium difficile* type 027/NAP1. J Clin Microbiol. 2008; 46:1530–1533. [PubMed: 18287318]

Barth H, Pfeifer G, Hofmann F, Maier E, Benz R, Aktories K. Low pH-induced formation of ion channels by *Clostridium difficile* toxin B in target cells. J Biol Chem. 2001; 276:10670–10676. [PubMed: 11152463]

Bartlett JG. Antibiotic-associated diarrhea. Clin. Infect. Dis. 1992; 15:9.

Bourgault AM, Lamothe F, Loo VG, Poirier L. the CDAD-CSI Study Group. In vitro susceptibility of *Clostridium difficile* clinical isolates from a multi-institutional outbreak in southern Quebec, Canada. Antimicrob Agents Chemother. 2006; 50:3473–3475. [PubMed: 17005836]

Burns DA, Heeg D, Cartman ST, Minton NP. Reconsidering the sporulation characteristics of hypervirulent *Clostridium difficile* BI/NAP1/027. PLoS One. 2011; 6:e24894. [PubMed: 21949780]

Carter GP, Douce GR, Govind R, Howarth PM, Mackin KE, Spencer J, et al. The anti-sigma factor TcdC modulates hypervirulence in an epidemic BI/NAP1/027 clinical Isolate of *Clostridium difficile*. PLoS Pathog. 2011; 7:e1002317. [PubMed: 22022270]

The Centers for Disease Control and Prevention. Surveillance for community-associated *Clostridium difficile*--Connecticut, 2006. Morb Mortal Wkly Rep. 2008:4.

Drudy D, Kyne L, O'Mahony R, Fanning S. *gyrA* mutations in fluoroquinolone-resistant *Clostridium difficile* PCR-027. Emerg Infect Dis. 2007; 13:2.

Drudy D, Quinn T, O'Mahony R, Kyne L, O'Gaora P, Fanning S. High-level resistance to moxifloxacin and gatifloxacin associated with a novel mutation in *gyrB* in toxin-A-negative, toxin-B-positive *Clostridium difficile*. J Antimicrob Chemother. 2006; 58:1264–1267. [PubMed: 17018563]

Egerer M, Giesemann T, Herrmann C, Aktories K. Auto-catalytic processing of *Clostridium difficile* toxin B - binding of inositol hexakisphosphate. J Biol Chem. 2009; 284:7.

Egerer M, Giesemann T, Jank T, Satchell KJF, Aktories K. Auto-catalytic cleavage of *Clostridium difficile* toxins A and B depends on cysteine protease activity. J Biol Chem. 2007; 282:25314–25321. [PubMed: 17591770]

Florin I, Thelestam M. Lysosomal involvement in cellular intoxication with *Clostridium difficile* toxin B. Microb Pathog. 1986; 1:373–385. [PubMed: 3508493]

Florin TM I. Internalization of *Clostridium difficile* cytotoxin into cultured human lung fibroblasts. Biochim Biophys Acta. 1983; 763:10.

Gerding D. Global epidemiology of *Clostridium difficile* infection in 2010. Infect Control Hosp Epidemiol. 2010; 31:S32–S34. [PubMed: 20929364]

Guttenberg G, Papatheodorou P, Genisyuerek S, Wei L, Jank T, Einsle O, Aktories K. Inositol hexakisphosphate-dependent processing of *Clostridium sordellii* lethal toxin and *Clostridium novyi* α-toxin. J Biol Chem. 2011; 286:14779–14786. [PubMed: 21385871]

Hamm EE, Voth DE, Ballard JD. Identification of *Clostridium difficile* toxin B cardiotoxicity using a zebrafish embryo model of intoxication. Proc Natl Acad Sci U S A. 2006; 103:14176–14181. [PubMed: 16966605]

Hirschhorn LR, Trnka Y, Onderdonk A, Lee MLT, Platt R. Epidemiology of community-acquired *Clostridium difficile*-associated diarrhea. J Infect Dis. 1994; 169:127–133. [PubMed: 8277174]

Irvine RF, Schell MJ. Back in the water: the return of the inositol phosphates. Nat Rev Mol Cell Biol. 2001; 2:12.

Just I, Selzer J, Wilm M, von Eichel-Streiber C, Mann M, Aktories K. Glucosylation of Rho proteins by *Clostridium difficile* toxin B. Nature. 1995; 375:500–503. [PubMed: 7777059]

Karas JA, Enoch DA, Aliyu SH. A review of mortality due to *Clostridium difficile* infection. J Infect. 2010; 61:1–8. [PubMed: 20361997]

Klein EJ, Boster DR, Stapp JR, Wells JG, Qin X, Clausen CR, et al. Diarrhea etiology in a children's hospital emergency department: A prospective cohort study. Clin Infect Dis. 2006; 43:807–813. [PubMed: 16941358]

Krivan HC, Wilkins TD. Purification of *Clostridium difficile* toxin A by affinity chromatography on immobilized thyroglobulin. Infect Immun. 1987; 55:1873–1877. [PubMed: 3112015]

Lanis JM, Barua S, Ballard JD. Variations in TcdB activity and the hypervirulence of emerging strains of *Clostridium difficile*. PLoS Pathog. 2010; 6:e1001061. [PubMed: 20808849]

Libby JM, Jortner BS, Wilkins TD. Effects of the two toxins of *Clostridium difficile* in antibiotic-associated cecitis in hamsters. Infect Immun. 1982; 36:822–829. [PubMed: 7085078]

McDonald LC, Killgore GE, Thompson A, Owens RC Jr, Kazakova SV, Sambol SP, et al. An epidemic, toxin gene-variant strain of *Clostridium difficile*. N Engl J Med. 2005; 353:2433–2441. [PubMed: 16322603]

McFarland LV, Mulligan ME, Kwok RYY, Stamm WE. Nosocomial acquisition of *Clostridium difficile* infection. N Engl J Med. 1989; 320:204–210. [PubMed: 2911306]

Merrigan M, Venugopal A, Mallozzi M, Roxas B, Viswanathan VK, Johnson S, et al. Human hypervirulent *Clostridium difficile* strains exhibit increased sporulation as well as robust toxin production. J Bacteriol. 2010; 192:4904–4911. [PubMed: 20675495]

Muto CA, Pokrywka M, Shutt K, Mendelsohn AB, Nouri K, Posey K, et al. A large outbreak of *Clostridium difficile*-associated disease with an unexpected proportion of deaths and colectomies at a teaching hospital following increased fluoroquinolone use. Infect Control Hosp Epidemiol. 2005; 26:273–280. [PubMed: 15796280]

Papatheodorou P, Zamboglou C, Genisyuerek S, Guttenberg G, Aktories K. Clostridial glucosylating toxins enter cells via clathrin- mediated endocytosis. PLoS One. 2010; 5:e10673. [PubMed: 20498856]

Pfeifer G, Schirmer J, Leemhuis J, Busch C, Meyer DK, Aktories K, Barth H. Cellular uptake of *Clostridium difficile* toxin B: translocation of the n-terminal catalytic domain into the cytosol of eukaryotic cells. J Biol Chem. 2003; 278:44535–44541. [PubMed: 12941936]

Pruitt RN, Chagot B, Cover M, Chazin WJ, Spiller B, Lacy DB. Structure-function analysis of inositol hexakisphosphate-induced autoprocessing in *Clostridium difficile* toxin A. J Biol Chem. 2009; 284:21934–21940. [PubMed: 19553670]

Puri AW, Lupardus PJ, Deu E, Albrow VE, Garcia KC, Bogyo M, Shen A. Rational design of inhibitors and activity-based probes targeting *Clostridium difficile* virulence factor TcdB. Chem Biol. 2010; 17:1201–1211. [PubMed: 21095570]

Qa'Dan M, Spyres LM, Ballard JD. pH-induced conformational changes in *Clostridium difficile* toxin B. Infect Immun. 2000; 68:2470–2474. [PubMed: 10768933]

Redelings MD, Sorvillo F, Mascola L. Increase in *Clostridium difficile*-related mortality rates, United States, 1999–2004. Emerg Infect Dis. 2007; 13:3.

Reineke J, Tenzer S, Rupnik M, Koschinski A, Hasselmayer O, Schrattenholz A, et al. Autocatalytic cleavage of *Clostridium difficile* toxin B. Nature. 2007; 446:415–419. [PubMed: 17334356]

Rupnik M, Pabst S, Rupnik M, von Eichel-Streiber C, Urlaub H, Soling HD. Characterization of the cleavage site and function of resulting cleavage fragments after limited proteolysis of *Clostridium difficile* toxin B (TcdB) by host cells. Microbiology. 2005; 151:199–208. [PubMed: 15632438]

Savidge TC, Urvil P, Oezguen N, Ali K, Choudhury A, Acharya V, et al. Host S-nitrosylation inhibits clostridial small molecule-activated glucosylating toxins. Nat Med. 2011; 17:1136–1141. [PubMed: 21857653]

Shen A, Lupardus PJ, Gersch MM, Puri AW, Albrow VE, Garcia KC, Bogyo M. Defining an allosteric circuit in the cysteine protease domain of *Clostridium difficile* toxins. Nat Struct Mol Biol. 2011; 18:364–371. [PubMed: 21317893]

Simor AE, Yake SL, Tsimidis K. Infection due to *Clostridium difficile* among elderly residents of a long-term-care facility. Clin Infect Dis. 1993; 17:672–678. [PubMed: 7903557]

Sorg JA, Sonenshein AL. Bile salts and glycine as cogerminants for *Clostridium difficile* spores. J Bacteriol. 2008; 190:2505–2512. [PubMed: 18245298]

Stabler R, He M, Dawson L, Martin M, Valiente E, Corton C, et al. Comparative genome and phenotypic analysis of *Clostridium difficile* 027 strains provides insight into the evolution of a hypervirulent bacterium. Genome Biol. 2009; 10:R102. [PubMed: 19781061]

Sullivan NM, Pellett S, Wilkins TD. Purification and characterization of toxins A and B of *Clostridium difficile*. Infect Immun. 1982; 35:1032–1040. [PubMed: 7068210]

Taylor NS, Thorne GM, Bartlett JG. Comparison of two toxins produced by *Clostridium difficile*. Infect Immun. 1981; 34:1036–1043. [PubMed: 7333662]

von Eichel-Streiber C, Sauerborn M, Kuramitsu HK. Evidence for a modular structure of the homologous repetitive C-terminal carbohydrate-binding sites of *Clostridium difficile* toxins and *Streptococcus mutans* glucosyltransferases. J Bacteriol. 1992; 174:6707–6710. [PubMed: 1307487]

Warny M, Pepin J, Fang A, Killgore G, Thompson A, Brazier J, et al. Toxin production by an emerging strain of *Clostridium difficile* associated with outbreaks of severe disease in North America and Europe. Lancet. 2005; 366:1079–1084. [PubMed: 16182895]

Wilcox MH, Mooney L, Bendall R, Settle CD, Fawley WN. A case control study of community-associated *Clostridium difficile* infection. J Antimicrob Chemother. 2008; 62:388–396. [PubMed: 18434341]

Wilson KH. Efficiency of various bile salt preparations for stimulation of *Clostridium difficile* spore germination. J Clin Microbiol. 1983; 18:1017–1019. [PubMed: 6630458]

Wilson KH, Sheagren JN, Freter R. Population dynamics of ingested *Clostridium difficile* in the gastrointestinal tract of the Syrian hamster. J Infect Dis. 1985; 151:355–361. [PubMed: 3968453]

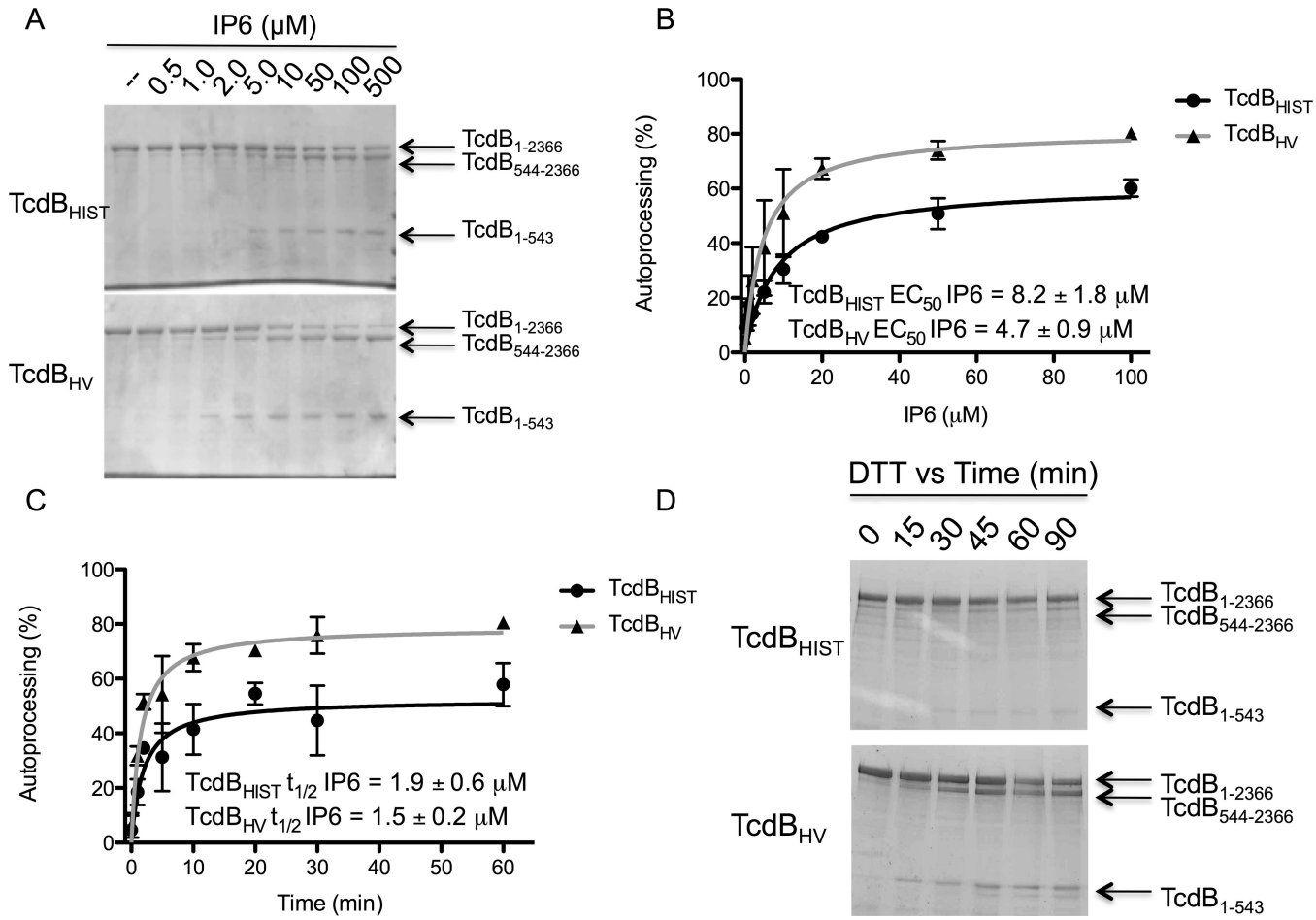

Fig. 1. In vitro processing of TcdB$_{HIST}$ and TcdB$_{HV}$ in response to inositol hexakisphosphate (IP6)

(A) Coomassie stained SDS-PAGE of TcdB$_{HIST}$ (top) or TcdB$_{HV}$ (bottom) that was treated with 500 nM to 500 μM of IP6. Full length TcdB (1-2366) and processed TcdB (544-2366 and 1-543) are indicated by the arrows. (B) Activation of autoprocessing by IP6. The percent autoprocessing of TcdB$_{HIST}$ (black) and TcdB$_{HV}$ (gray) was determined by comparing the relative amounts of TcdB$_{1-543}$ and TcdB$_{544-2366}$ to full-length toxin using densitometry. The activation constant (EC50), is defined as the concentration of IP6 at which half-maximal activity occurs. Error bars represent the S.D. of 4 independent experiments and toxin preparations. (C) Comparison of the rate of TcdB processing in response to IP6. TcdB$_{HIST}$ or TcdB$_{HV}$ were incubated with 100 μM of IP6 for the time points indicated and the reactions resolved by SDS-PAGE. The percent autoprocessing of TcdB$_{HIST}$ (black) and TcdB$_{HV}$ (gray) was determined by comparing the relative amounts of TcdB$_{1-543}$ and TcdB$_{544-2366}$ to full-length toxin using densitometry. The time to half-max ($t_{1/2}$), is defined as the time at which half-maximal activity occurs. Error bars represent the S.D. of 4 independent experiments and toxin preparations. (D) Coomassie stained SDS-PAGE of TcdB$_{HIST}$ (top) or TcdB$_{HV}$ (bottom) that was treated with 5 mM DTT for up to 90 min. Full length TcdB (1-2366) and processed TcdB (544-2366 and 1-543) are indicated by the arrows.

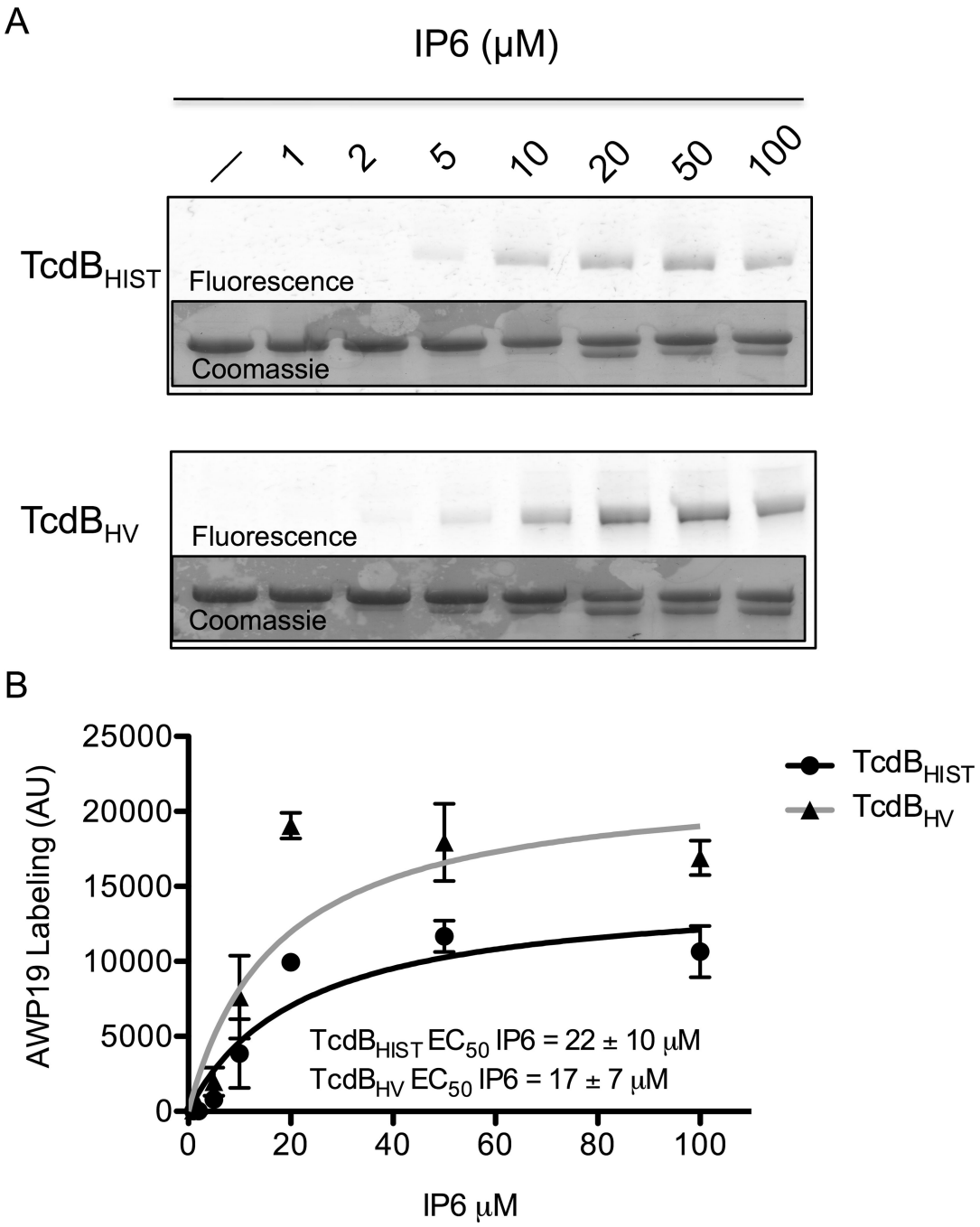

Fig. 2. Comparison of cysteine protease activation with the activity-based probe AWP19

(A) Representative fluorescent gel image of the IP6 induced labeling of TcdB$_{HIST}$ (top) or TcdB$_{HV}$ (bottom) by AWP19. The in vitro cleavage assay was allowed to come to completion with the indicated concentration of IP6, then the gel was imaged for FITC fluorescence. Inset: Coomassie stained gel verifying equal loading. (B) Densitometry indicating the average fluorescence intensity (arbitrary units) of TcdB$_{HIST}$ (black) and TcdB$_{HV}$ (gray) at the indicated IP6 concentrations. The activation constant (EC50), is defined as the concentration of IP6 at which half-maximal activity occurs. Error bars represent the S.D. of 4 independent experiments.

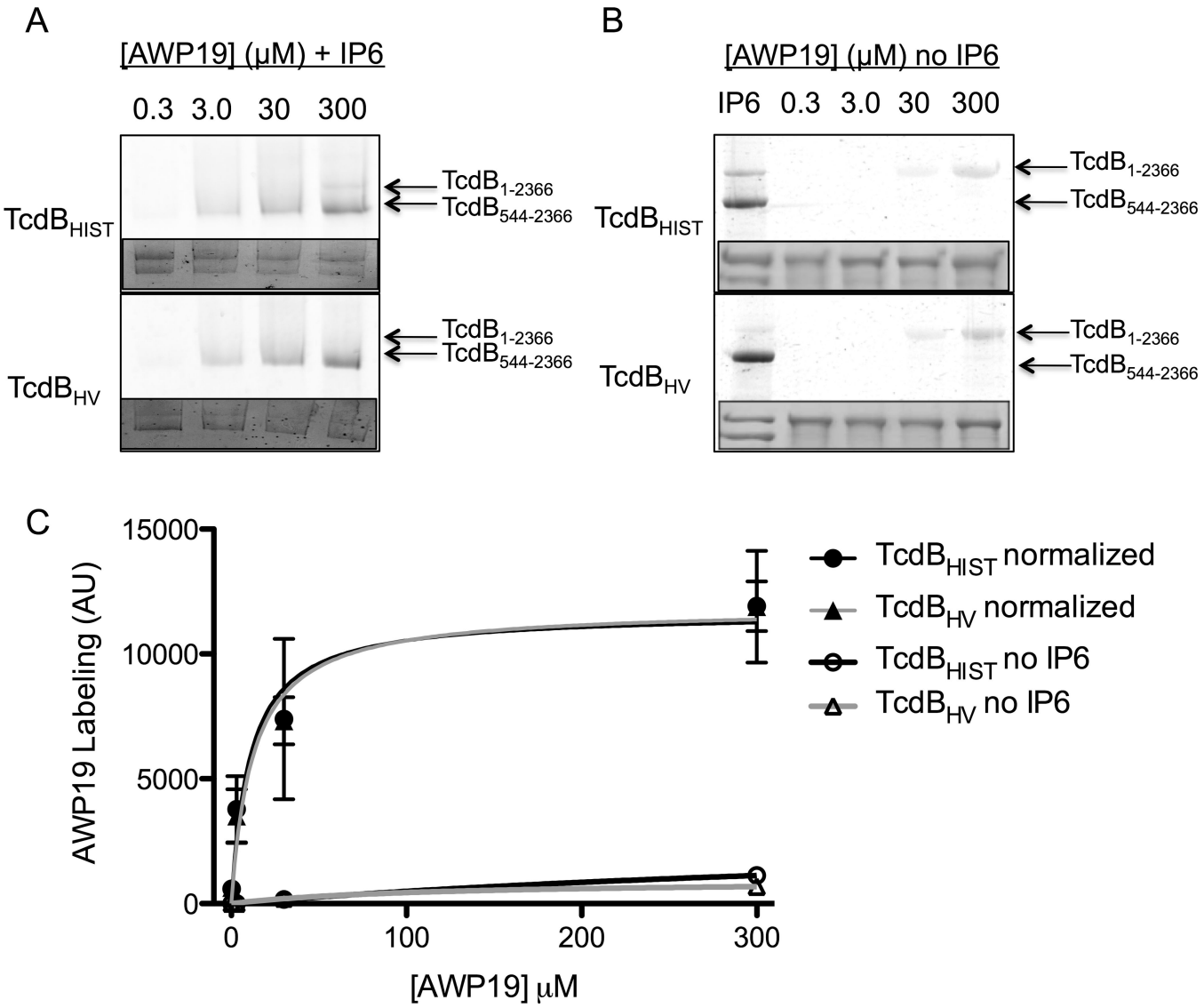

Fig. 3. AWP19 probe binding affinity

(A) Representative fluorescent gel image of the IP6 induced labeling of TcdB$_{HIST}$ (top) or TcdB$_{HV}$ (bottom) in response to AWP19 concentration. The in vitro cleavage assay was allowed to come to completion in the presence of 100 μM IP6, then the gel was imaged for FITC fluorescence. (B) Representative fluorescent gel image of the labeling of TcdB$_{HIST}$ (top) or TcdB$_{HV}$ (bottom) in response to AWP19 alone. The probe indicated concentration of probe was incubated with 0.3 μM of TcdB overnight, then the gel was imaged for FITC fluorescence. The lane marked IP6 indicateds the control in which IP6 was included. (C) Densitometry indicating the average fluorescence intensity (arbitrary units) of TcdB$_{HIST}$ (black) and TcdB$_{HV}$ (gray) at the indicated AWP19 concentrations which has either been normalized to the percent processing or incubated without IP6. Error bars represent the S.D. of triplicate samples.

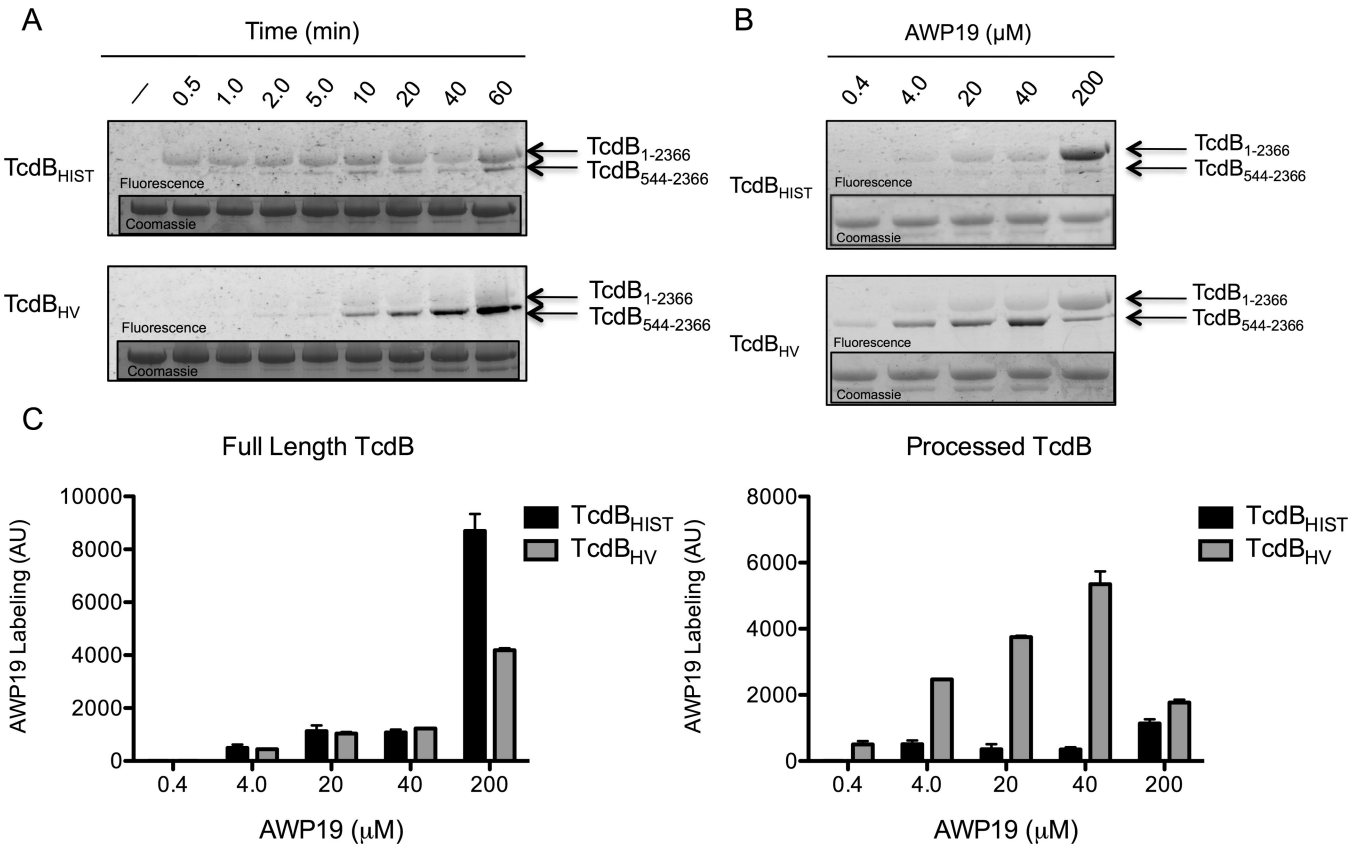

Fig. 4. AWP19 labeling of TcdB in response to rate of IP6 activation and AWP19 probe concentration

(A) Representative fluorescent gel image of the AWP19 labeling at the indicated time points after activation of 0.5 μM of $TcdB_{HIST}$ (top) or $TcdB_{HV}$ (bottom) with 25 μM IP6. Full length TcdB (1-2366) and processed TcdB (544-2366) are indicated by the arrows. Inset: Coomassie stained gel verifying equal loading. (B) Representative fluorescent gel image of AWP19 labeling in response to increasing concentrations of the fluorescent probe. 0.4 μM of $TcdB_{HIST}$ (top) or $TcdB_{HV}$ (bottom) were incubated simultaneously with 25 μM of IP6 and the indicated concentration of AWP19 for 1 h. Full lengths TcdB (1-2366) and processed TcdB (544-2366) are indicated by the arrows. Inset: Coomassie stained gel verifying equal loading. (C) Densitometry indicating the average fluorescence intensity (arbitrary units) of $TcdB_{HIST}$ (black) and $TcdB_{HV}$ (gray) at the indicated AWP19 concentrations. Error bars represent the S.E.M. of triplicate samples.

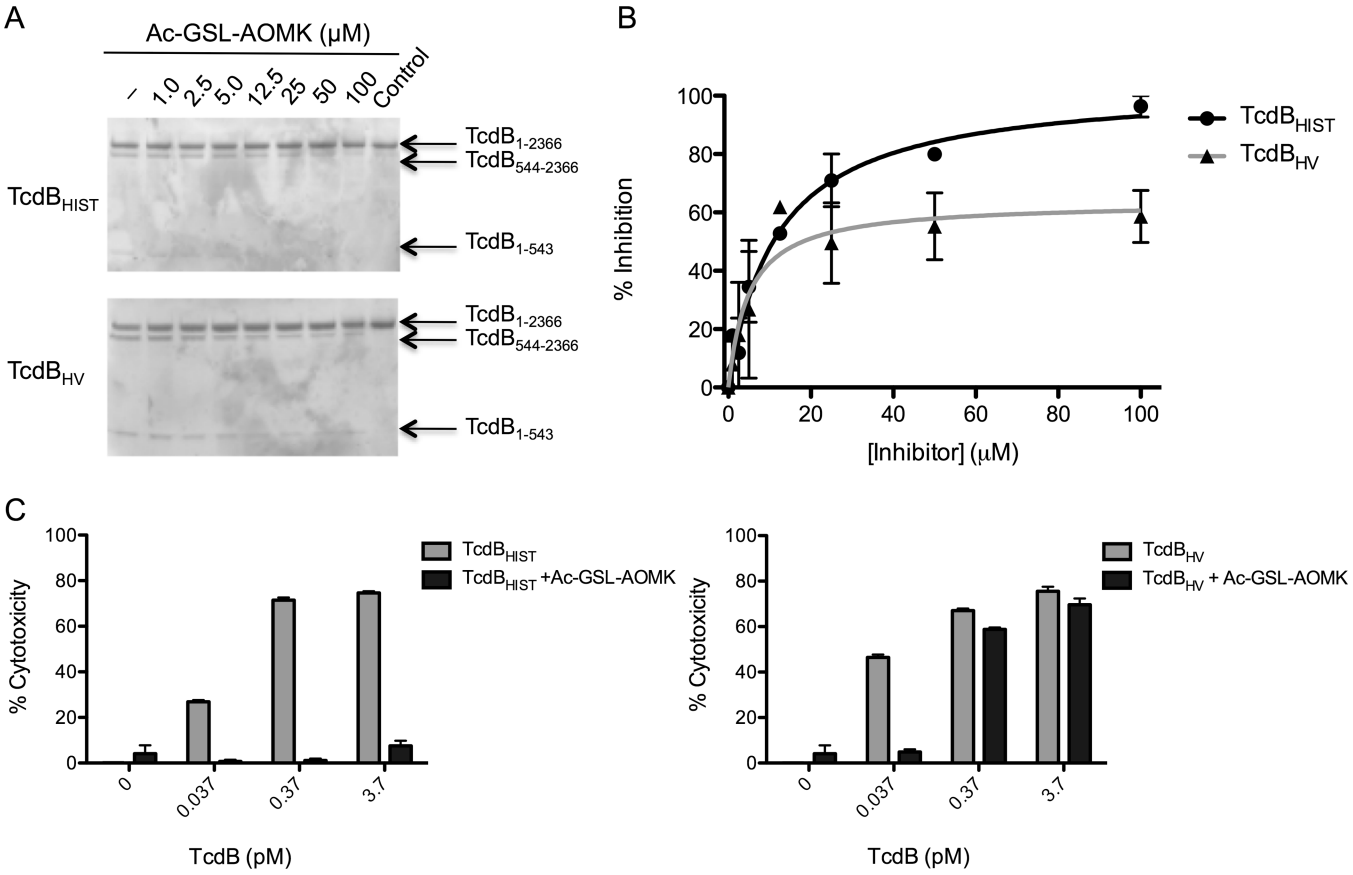

Fig. 5. Chemical inhibition of the TcdB CPD with Ac-GSL-AOMK

(A) 2.5 μg of $TcdB_{HIST}$ (top) or $TcdB_{HV}$ (bottom) were pre-incubated with 1 μM to 100 μM of Ac-GSL-AOMK for 1 h. Then 25 μM IP6 was added and the samples were incubated for 1 h and separated by SDS-PAGE. Full length TcdB (1-2366) and processed TcdB (544-2366 and 1-543) are indicated by the arrows. (B) Quantification of the percentage of inhibition of $TcdB_{HIST}$ (black) and $TcdB_{HV}$ (gray) as determined by densitometry. (C) CHO cell cytotoxicity of $TcdB_{HIST}$ (left) or $TcdB_{HV}$ (right) that have been treated with 100 μM of the CPD inhibitor Ac-GSL-AOMK. Error bars represent the S.E.M. of triplicate samples.

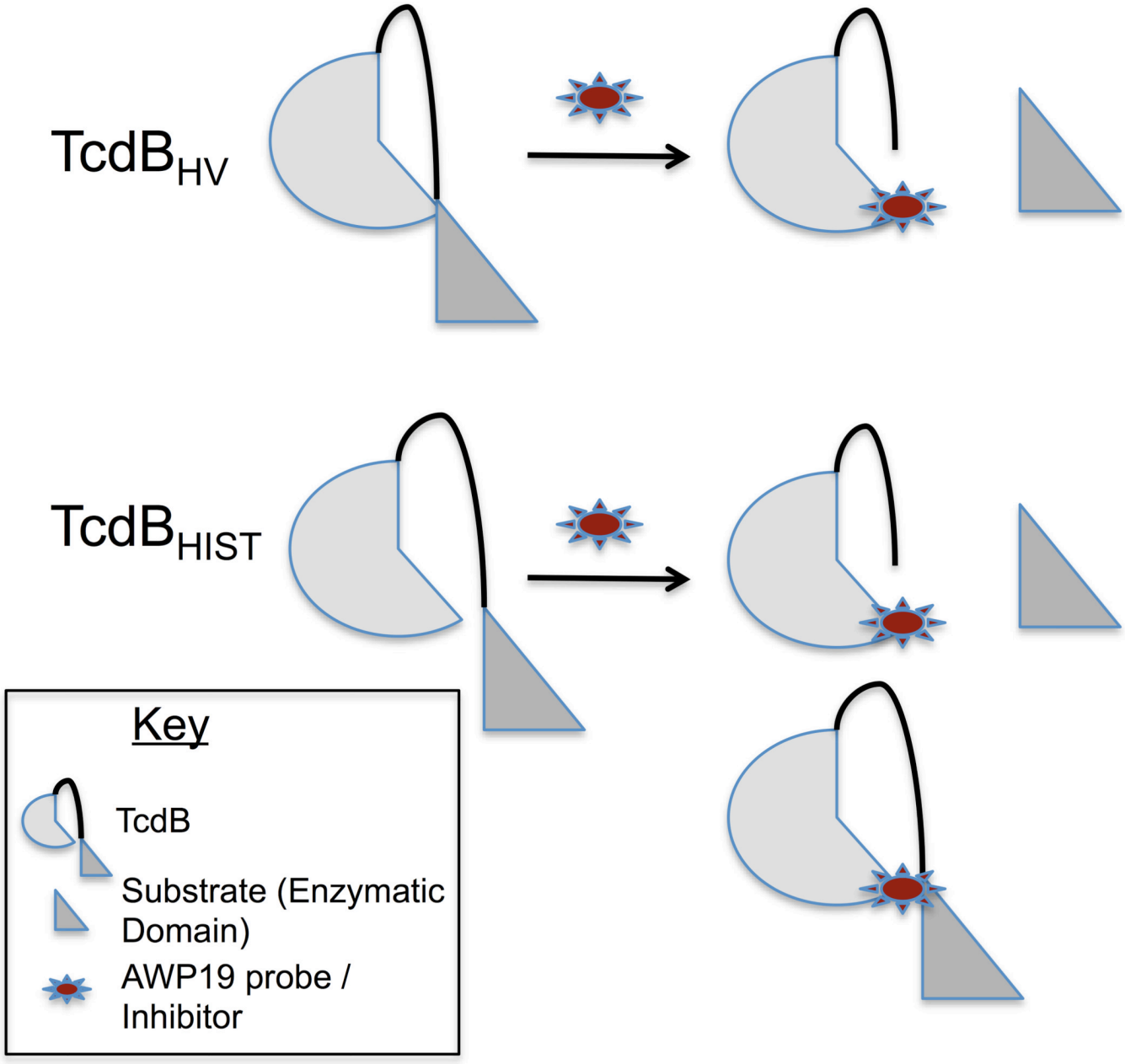

Fig. 6. Intramolecular interactions of TcdB$_{HIST}$ and TcdB$_{HV}$

A working model demonstrating the fundamental differences in the CPD conformation and activity between TcdB$_{HIST}$ and TcdB$_{HV}$. TcdB$_{HV}$ (top) undergoes an intramolecular interaction that precludes binding to the probe until after substrate is cleaved. The intramolecular reaction of TcdB$_{HIST}$ (bottom) is not sufficient to block binding by the probe, thus cleaved and uncleaved toxin can be labeled.